Michaud *et al.*
Journal of NeuroEngineering and Rehabilitation (2025) 22:156
https://doi.org/10.1186/s12984-025-01691-z

Journal of NeuroEngineering and Rehabilitation

RESEARCH

Open Access

Comparison of subject-specific musculoskeletal model calibration strategies on muscle force and fatigue estimation

Florian Michaud[1*], Gonzalo Márquez[2], Manuel A. Giraldez-García[3] and Javier Cuadrado[1]

Abstract

Muscle force and fatigue modeling and simulation are powerful tools for rehabilitation, sports performance, ergonomics, and injury prevention. However, their accuracy is challenged by dynamic mechanical and physiological factors. Since musculoskeletal models are typically derived from cadaver data and scaled to individuals, careful subject-specific calibration is recommended to achieve accurate simulation results. This study investigates how different muscle models and calibration strategies affect the accuracy of muscle force estimation at the elbow level. Two models—a simplified static model and a rigid-tendon Hill-type model—were compared. Several calibration approaches were tested using isometric and isokinetic measurements to identify the parameters that most enhance model performance. The models were used to estimate muscle forces, and their outputs were compared to experimental data collected from seventeen healthy subjects. In the first phase, estimations were made during short maximal voluntary contractions (MVCs) without fatigue, in order to isolate muscle force from fatigue effects. In the second phase, the calibrated parameters from each strategy were used to estimate muscle forces and fatigue during a short-duration, high-intensity dynamic exercise by incorporating a muscle fatigue model. The highest accuracy was achieved with the Hill-type model, which involved refining individual muscle length and force parameters based on concentric and eccentric MVCs and adjusting two parameters of the force–velocity relationship. However, incorporating subject-specific muscle fatigue parameters did not significantly improve force estimation under fatigue conditions.

Keywords Muscle force dynamics, Muscle fatigue model, Biomechanics, Musculotendon model, Rehabilitation, Sport performance

*Correspondence:
Florian Michaud
florian.michaud@udc.es
[1] Laboratory of Mechanical Engineering, CITENI, Campus Industrial de Ferrol, Universidade da Coruña, Ferrol, Spain
[2] Department of Physical Education and Sport, Faculty of Sports Sciences and Physical Education, Universidade da Coruña, A Coruña, Spain
[3] Performance and Health Group, Faculty of Sport Sciences and Physical Education, Universidade da Coruña, A Coruña, Spain

Introduction

Estimating muscle forces through computer modeling and simulation is a powerful tool for evaluating joint loads and muscle fatigue, with applications in rehabilitation, physical therapy, human motion prediction, athletic performance optimization, ergonomic design, and injury prevention in both sports and workplaces [1–7]. These simulations are especially valuable in scenarios where direct measurement of internal forces is impractical or impossible [8]. However, accurately modeling muscle forces remains a significant challenge due to the inherently dynamic and nonlinear nature of musculoskeletal systems [9–11]. Muscle tendon units (MTU) force generation varies over time and is sensitive to a multitude of mechanical and physiological factors such as moment arms, tendon lengths, activation patterns, and the progression of muscle fatigue [12–14]. Currently, generating a musculoskeletal model directly from medical images is not technically feasible; instead, generic models are derived from cadaver data and adjusted to fit individual subjects using basic scaling methods [15]. While this approach can provide a rough estimate of musculoskeletal geometry, it lacks the precision needed for high-fidelity force estimation. Since MTU force output is highly dependent on individualized anatomical and physiological properties, relying solely on generic models risks oversimplification and inaccuracy, particularly in sensitive applications like rehabilitation planning or elite athletic performance assessment.

To improve simulation accuracy, it is therefore essential to move toward subject-specific modeling approaches that incorporate calibrated parameters. Calibration techniques help tailor musculoskeletal models to better reflect individual variability, enhancing the physiological realism of simulated musculotendon mechanics [16]. These techniques become even more crucial when working with sophisticated MTU models that include a greater number of adjustable parameters, each of which can significantly influence force output predictions. Traditional MTU force inputs—such as musculotendon length, shortening velocity, and moment arms—are dictated by joint kinematics and musculoskeletal geometry. However, other critical parameters like optimal MTU fiber length and tendon slack length can only be approximated through indirect methods such as anthropometric scaling [17, 18]. Moreover, dynamic simulations that aim to capture force–time behavior require further tuning of parameters such as maximum isometric force and fatigue/recovery coefficients. These latter parameters are particularly relevant when modeling conditions involving sustained exertion or repetitive motion, where muscle fatigue plays a significant role [19, 20]. For example, in rehabilitation contexts, understanding the fatigue profile of a patient can inform therapy intensity and rest cycles [21–23]. Similarly, in sports science, incorporating fatigue dynamics can improve performance modeling and reduce injury risk during training [24–26]. Thus, parameter calibration is not merely a technical refinement but a necessary step toward achieving accurate, personalized, and context-sensitive musculoskeletal simulations [27].

In their preliminary study on integrating muscle force and muscle fatigue simulation, the authors highlighted the challenges of obtaining accurate subject-specific human models for dynamic tasks [28]. They successfully combined multilevel models that account for redundant muscle forces within a multibody environment with muscle fatigue; however, they observed discrepancies with experimental values due to the muscle fatigue model used and the calibration of MTU parameters. In their subsequent work, they developed an innovative four-compartment model that distinguishes between short-term fatigue (related to metabolic inhibition) and long-term fatigue (emulating central fatigue and potential microtraumas), validating it exclusively during isometric tasks to correctly isolate the fatigue mechanism and avoid the dynamic effects of complex MTU force generation [29]. Later, Yang et al. proposed a specific muscle fatigue model for both static and dynamic tasks, using an isokinetic dynamometer to establish generic model parameters [30]. However, their study focused solely on concentric contractions and did not incorporate MTU force mechanisms, which are crucial for fatigue estimation as they determine the target load of a physical activity (the key input for any muscle fatigue model). On the other hand, Thelen extensively studied MTU force modeling, paying particular attention to adjusting MTU mechanics parameters to simulate dynamic contractions [31]. He also used an isokinetic dynamometer to determine the Hill-muscle model parameters [32] that best fit specific population groups, highlighting subject-specific discrepancies and their impact on MTU force production. Other authors [33–35] proposed calibration strategies for their musculoskeletal models based on motion capture, electromyography measurements and ground forces data. Muller et al. calibrated geometric parameters from motion capture and also used an isokinetic dynamometer for MTU force calibration, but only during isometric trials [27]. Finally, while none of these studies considered the effect of musculoskeletal model personalization on muscle fatigue, Arones et al. investigated its impact on metabolic cost estimates during walking [36].

For these reasons, this study aims to enhance muscle force and fatigue estimation by comparing different MTU models and calibration strategies. Specifically, the authors explore the impact of MTU model types and calibration techniques on the precision of MTU force estimation at the elbow joint. Two modeling approaches were evaluated: a basic static model and a more detailed rigid-tendon Hill-type model. Multiple calibration methods were applied using data from isometric and isokinetic tests to determine which parameters most effectively improve model accuracy. These models were then used to compute MTU forces and validated against experimental data obtained from seventeen healthy participants. The evaluation was conducted in two stages. Initially, predictions were made during brief maximal voluntary contractions (MVCs) under non-fatigued conditions, aiming to assess pure muscle force. In the subsequent stage, the models—now calibrated—were used to simulate both muscle force and fatigue during a short, high-intensity dynamic task, using a fatigue model.

Material and methods

Experimental data collection

Participants and instrumentation

Seventeen healthy voluntary participants (8 males, 9 females; age: 32 ± 13 years; height: 175 ± 18 cm; body mass: 72 ± 20 kg) were recruited for this study. Inclusion criteria were: (i) self-reported good general health, (ii) no history of upper limb musculoskeletal injuries or neuromuscular disorders, and (iii) ability to perform maximal voluntary elbow flexions without pain or discomfort. Exclusion criteria included: (i) current upper limb pain or injury, (ii) recent engagement in upper-body strength training within 48 h before testing, and (iii) consumption of caffeine, alcohol, or participation in vigorous physical activity within the same 48-h period. Before participating, each individual provided written informed consent, which had been approved by the Research Ethics Committee of La Coruña-Ferrol. The subjects' arm, forearm, and hand were measured to later scale the subject-specific models.

The HUMAC Norm isokinetic dynamometer (CSMi, Stoughton, MA, sampled at 100 Hz) was used to record joint angle and torque generated by the participants. Each subject was positioned in a lying posture and securely restrained to ensure that only the right elbow could move, as shown in Fig. 1a.

Experimental procedures

Participants followed both an isometric and an isokinetic exercise protocol on the same day. At the start of the session, they completed a 5-min warm-up using a resistance band to reduce the risk of injury. To ensure familiarity with the evaluations and instructions, a simulated recording was made beforehand for each task. Task-specific guidelines, including the number of repetitions, pace, and rest periods, were provided both verbally and visually on a screen positioned next to the subject. During all exercises, participants were instructed to exert maximum voluntary contraction (MVC) and received verbal encouragement throughout [37].

The isometric exercise protocol (hereafter referred to as ISOM6) began with two MVCs, each held for 5 s, at six different elbow flexion angles (15°, 30°, 45°, 60°, 75°, and 90°) in a randomized order. The higher peak force of the two MVCs was retained, and the difference between the two MVCs was checked to ensure it did not exceed 10%. A 45-s rest period was given between the two MVCs of each angle, and a 2-min rest between the MVCs of different angles to minimize the effects of muscle fatigue. After a 5-min rest, participants performed a 30-s sustained MVC at 45°, followed by two additional 5-s MVCs, with rest intervals of 15 s and 60 s, respectively, to measure recovery. Since this exercise induced metabolic inhibition, participants were given a minimum of 30 min of rest before proceeding with the isokinetic protocol.

The isokinetic exercise protocol began with two MVCs during concentric elbow flexion from 15° to 90° at a speed of 15°/s (5 s duration). This ensured

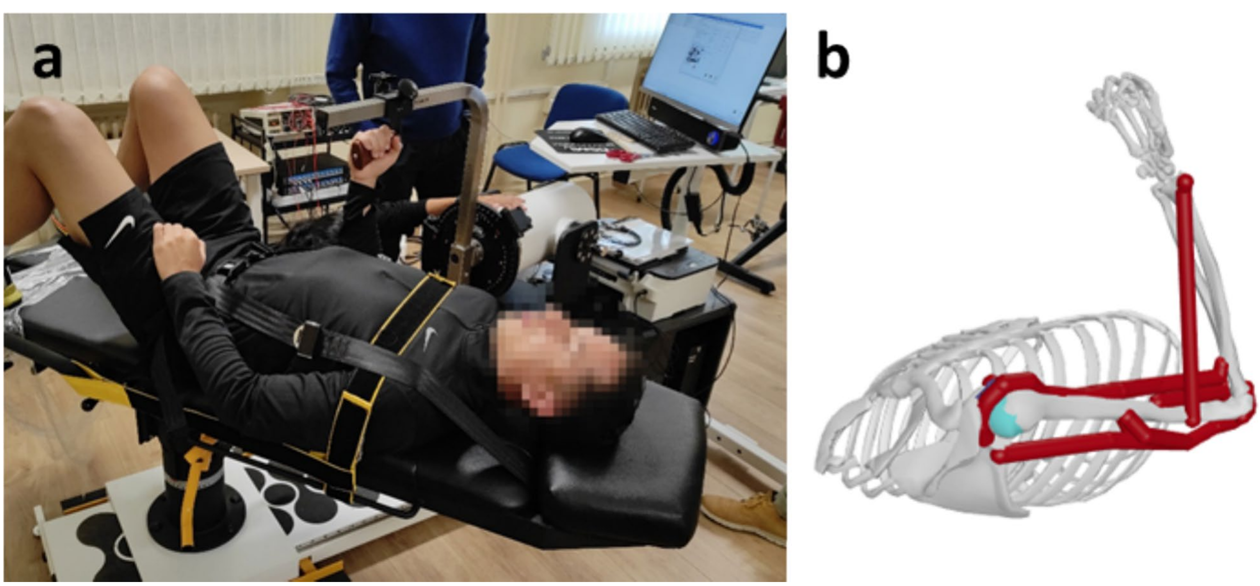

Fig. 1 **a** Isokinetic dynamometer; **b** 7-muscle arm model

participants exerted maximum force throughout the entire range of motion, without fatiguing and allowing the dynamometer to accurately measure it. Additionally, the initial 10° of both eccentric and concentric contractions were excluded from calibration to avoid the effects of the muscle's response time to excitation. Next, subjects performed two MVCs during eccentric elbow flexion, where they resisted the machine as it extended their arm from 90° to 15° at the same speed and duration. The speed of this exercise not only aimed to achieve maximum effort like the previous one, but also served to reduce the risk of injury, as the machine exerts significant torque. For both exercises, a 45-s rest period was given between each MVC, with a 2-min rest between the two sets. The four sets of measurements (two concentric and two eccentric) were later used in the simulation, and the protocol is referred to as DYN. Finally, after a 5-min rest, participants performed a dynamic, short-duration, high-intensity exercise (DYN-FAT). This involved sustaining an MVC during 4 concentric (15°–90°) and eccentric (90°–15°) elbow flexions (40-s total duration), followed by two additional 5-s isometric MVCs at 45°, with 15-s (DYN-FAT-R1) and 60-s (DYN-FAT-R2) rest intervals, respectively, to measure recovery.

Models

Musculoskeletal model

The musculoskeletal model used in this study consisted of four segments—trunk, upper arm, forearm, and hand—with a single degree of freedom, allowing only elbow flexion and extension (Fig. 1b). All other joints were fixed and set to match the subject's posture during the experimental setup (Fig. 1a, b). It incorporated seven muscles: the long, medial, and lateral heads of the triceps; the long and short heads of the biceps; the brachioradialis; and the brachialis. Adapted from [38], the bone geometries were scaled to match each subject's anthropometric measurements. By combining this model with the recorded joint angles from the isokinetic dynamometer, MTU lengths and moment arms were determined for the exercises.

Musculotendon models

Two types of musculotendon models were used to estimate MTU force. The first was a Hill-type musculotendon model [32] (Fig. 2), which accounts for physiological force constraints. The force generated by a MTU depends on its maximum isometric force, as well as its force–length-velocity properties, and is provided by:

$$F^{MT} = \left(F^{M}_{CE} + F^{M}_{PE}\right)\cos\alpha; \tag{1}$$

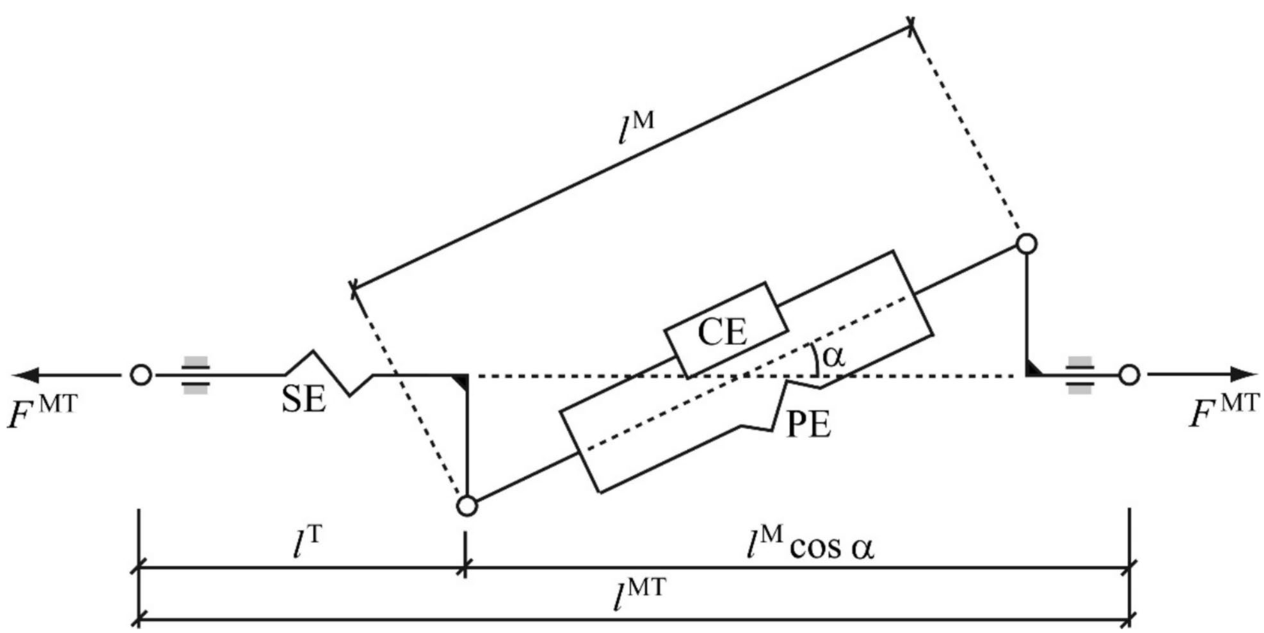

Fig. 2 Hill-type musculotendon model. The MTU fibers are modeled as an active contractile element (CE) in parallel with a passive elastic component (PE). These elements are in series with a nonlinear elastic tendon (SE). The pennation angle α denotes the angle between the MTU fibers and the tendon. Superscripts MT, M, and T indicate musculotendon, MTU fiber, and tendon, respectively [28]

In this equation, F_{CE}^{M} and F_{PE}^{M} represent the forces generated by the contractile element (CE) and the passive element (PE), respectively, while α corresponds to the pennation angle. The active force produced by the CE is influenced by MTU fiber length, contraction velocity, and activation level, and is defined as:

$$F_{CE}^{M} = F_0^{M} \times a \times f_l\left(l^{M}\right) \times f_v\left(v^{M}\right); \tag{2}$$

where l^M is the MTU fiber length, v^M is its velocity, and f_l and f_v are dimensionless force–length and force–velocity relationships, respectively. Since the authors aim to integrate the findings of this study into their real-time human motion capture and musculoskeletal analysis system [39], the tendon is assumed to be rigid, meaning that its length remains constant. This assumption reduces the numerical stiffness of the Hill-muscle equations [40, 41], and significantly decreases the computational time required for simulations while preserving the key physiological considerations [42]. As a result, MTU fiber length and velocity are determined solely by musculoskeletal geometry and segment motion, independently of the musculotendon force. Moreover, to further achieve this objective, the muscle's time response to excitation is ignored, assuming that activation follows excitation instantaneously, where activation a equals excitation u. This simplification is justified by the fact that the time delays involved are minimal compared to the duration of the exercises analyzed—muscles had sufficient time to reach maximum activation—and, in the context of fatigue, the effect of activation delays would be largely compensated by the corresponding deactivation delays. In Fig. 2, l^{MT} stands for the musculotendon length and v^{MT} is the musculotendon velocity.

The force of the parallel passive element, F_{PE}^{M}, which opposes MTU stretch, can be formulated as:

$$F_{PE}^{M} = F_0^{M} \times f_{PE}\left(l^{M}\right); \tag{3}$$

where f_{PE} is a dimensionless force–length relationship, which has non-zero values when the MTU length is greater than the optimal MTU fiber length (l_0^M).

In this study, subjects were instructed to produce their MVC to avoid the load-sharing problem. Without this approach, it would be impossible to calibrate maximum forces and determine whether variations in experimental torques were caused by muscle fatigue or by voluntary reductions in muscular activity. Therefore, the activation of the elbow flexors was assumed to be 1 (maximum), while the activation of the elbow extensors was set to 0 (minimum, with no co-contractions). Consequently, the instantaneous allowed forces in flexor and extensor muscles, F^{Flex} and F^{Ext}, were calculated using $a=1$ (maximal active contraction) and $a=0$ (no active contraction), respectively. In this way, by combining Eqs. (1–3), the resulting flexor and extensor single MTU forces, F_i^{Flex} and F_i^{Ext}, in muscle i, are represented by Eqs. (4) and (5), respectively.

$$F^{Flex} = \left(f_l\left(l^{M}\right) \times f_v\left(v^{M}\right) + f_{PE}\left(l^{M}\right)\right)F_0^{M} \times \cos\alpha; \tag{4}$$

$$F^{Ext} = f_{PE}\left(l^{M}\right) \times F_0^{M} \times \cos\alpha; \tag{5}$$

The second model was a simplified static model that does not account for musculotendon actuator dynamics. In this model, the musculotendon force (F_{Stat}^{MT}) is directly related to MTU activation (a) and maximum isometric force (F_0^M):

$$F_{Stat}^{MT} = a \times F_0^{M}; \tag{6}$$

Consequently, using the static model, the force of flexor MTUs is $F_{Stat}^{Flex} = F_0^M$ and the force of extensor MTUs is $F_{Stat}^{Ext} = 0$ during elbow flexion MVC. Due to its simplicity, this model only requires the calibration of the maximum isometric force and offers good computational efficiency. Moreover, it has not shown significant differences compared to more physiologically realistic models during gait [42].

Muscle fatigue model

Muscle fatigue is a complex phenomenon influenced by both physiological and psychological factors, leading to a reduced ability to generate maximal force or power during contractile activity. It can occur at different levels of the motor pathway, and is generally classified into central and peripheral fatigue. Central fatigue refers to a decline in the central nervous system's ability to transmit neural signals to the muscles, resulting in diminished muscle performance [43]. In contrast, peripheral fatigue occurs at the neuromuscular junction and within the muscle itself, involving mechanical and cellular alterations [44]. The recovery of voluntary force-generating capacity after exercise varies, with brief high-intensity exercise typically allowing for rapid recovery, and long-duration exercise often resulting in only partial recovery [45]. To simulate the task-related muscle fatigue for dynamic movements, this work implements a compartment model to characterize muscle activation (M_a), fatigue (M_f), and recovery (M_r) across any target load (TL) [46]. Specifically, the authors adopted the innovative four-compartment (4CC) model which differentiates between short-term fatigue (M_f^S, associated with metabolic inhibition) and long-term fatigue (M_f^L, simulating central fatigue and potential microtraumas) [29]. The portion of each subject's maximum force available at the joint level reflects the proportion of non-fatigued MTUs (RC), accounting for both short-term and long-term fatigue. It is expressed as:

$$RC = \left(100 - \left(M_f^S + M_f^L\right)\right)/100; \tag{7}$$

Consequently, accounting for fatigue, the maximum force that the flexor MTUs can generate within the static musculotendon model during MVC ($a=1$) can be expressed as:

$$F_{Stat}^{MT} = F_0^M \times RC; \tag{8}$$

Then, considering that peripheral and central fatigue primarily affect the contractile component of MTU force production, only F_{CE}^M (2) will be influenced by the muscle's fatigue level. Consequently, the reduction in maximum MTU force permitted in the elbow flexor MTU during MVC within the physiological model can be formulated as follows:

$$\begin{aligned} F^{Flex} = &\left(f_l\left(l^M\right) \times f_v\left(v^M\right) \times RC + f_{PE}\left(l^M\right)\right) \\ &\times F_0^M \times \cos\alpha; \end{aligned} \tag{9}$$

Torque calculation

The net elbow joint torque at each moment during the tasks can be expressed, in a general form, as:

$$J^T F^{MT} = Q; \tag{10}$$

where $\mathbf{F}^{MT}$ is the vector of the individual MTU forces, $\mathbf{J}$ is the Jacobian whose transpose projects the MTU forces into the joint drive torque space (i.e., represents the moment arms), and Q is the resulting elbow joint torque.

The experimental joint torque (Q_{Exp}) was directly recorded using the isokinetic dynamometer.

Subject-specific scaling or calibration of musculotendon parameters

Since mechanical and physiological factors influence MTU forces during joint angle variations, three different datasets were compared for calibration:

- A single isometric MVC at 60° (ISOM1).
- Six static experimental measurements of isometric MVCs (ISOM6).
- An isokinetic calibration task, including both concentric and eccentric contractions (DYN).

The following musculotendon parameters have been calibrated or optimized in this study:

Maximum isometric force

Since the relative target load of a task depends on the force exerted by the subject, the maximum isometric force (F_0^M) is one of the most critical subject-specific parameters to calibrate. In most studies, this parameter is adjusted to ensure that MTUs can generate the required joint torques [35, 47], sometimes by artificially increasing F_0^M or incorporating residual actuators into the model. According to the OpenSim documentation, these residual actuators are referred to as "the hand of God," as they compensate for discrepancies between model, recorded movements and MTU forces that fail to produce sufficient accelerations [48]. In fatigue studies, overestimating F_0^M leads to an underestimation of fatigue, while underestimating it exaggerates fatigue effects. Therefore, correct calibration of F_0^M is essential to accurately approximate the subject's force and fatigue limits, ensuring that MTU forces can generate the required joint torques without being underactivated.

Since the variation of MTU moment arms across joint angles differs among muscles, optimizing individual MTU forces provides greater flexibility for the model to align with experimental measurements without altering the moment arms. Modifying moment arms would require adjusting the coordinates of MTU and tendon attachment sites, leading to significant structural changes and collateral consequences.

Length parameters

The scaled tendon slack length (l_S^T) and the scaled optimal MTU fiber length (l_0^M), which influence the dimensionless force–length function, were obtained from OpenSim [38] after adjusting the model to match anthropometric measurements. Nevertheless, to determine the best subject-specific calibration strategy, a second scaling was also applied to l_0^M by including this parameter in the list of variables to optimize in ISOM6 and DYN.

Additional force–length-velocity properties

Preliminary results using the Hill muscle model (original model, shown in orange in Fig. 3) indicated that none of the implemented and calibrated approaches accurately captured the experimental MTU force–length and force–velocity relationships. This discrepancy was observed across both dynamic and isometric protocols, with two eccentric and two concentric MVCs highlighted in red and six isometric MVCs in green in Fig. 3. Two key observations emerged:

a. The experimental measurements and previous findings in [49] indicate that concentric contractions are most affected by musculotendon length-velocity

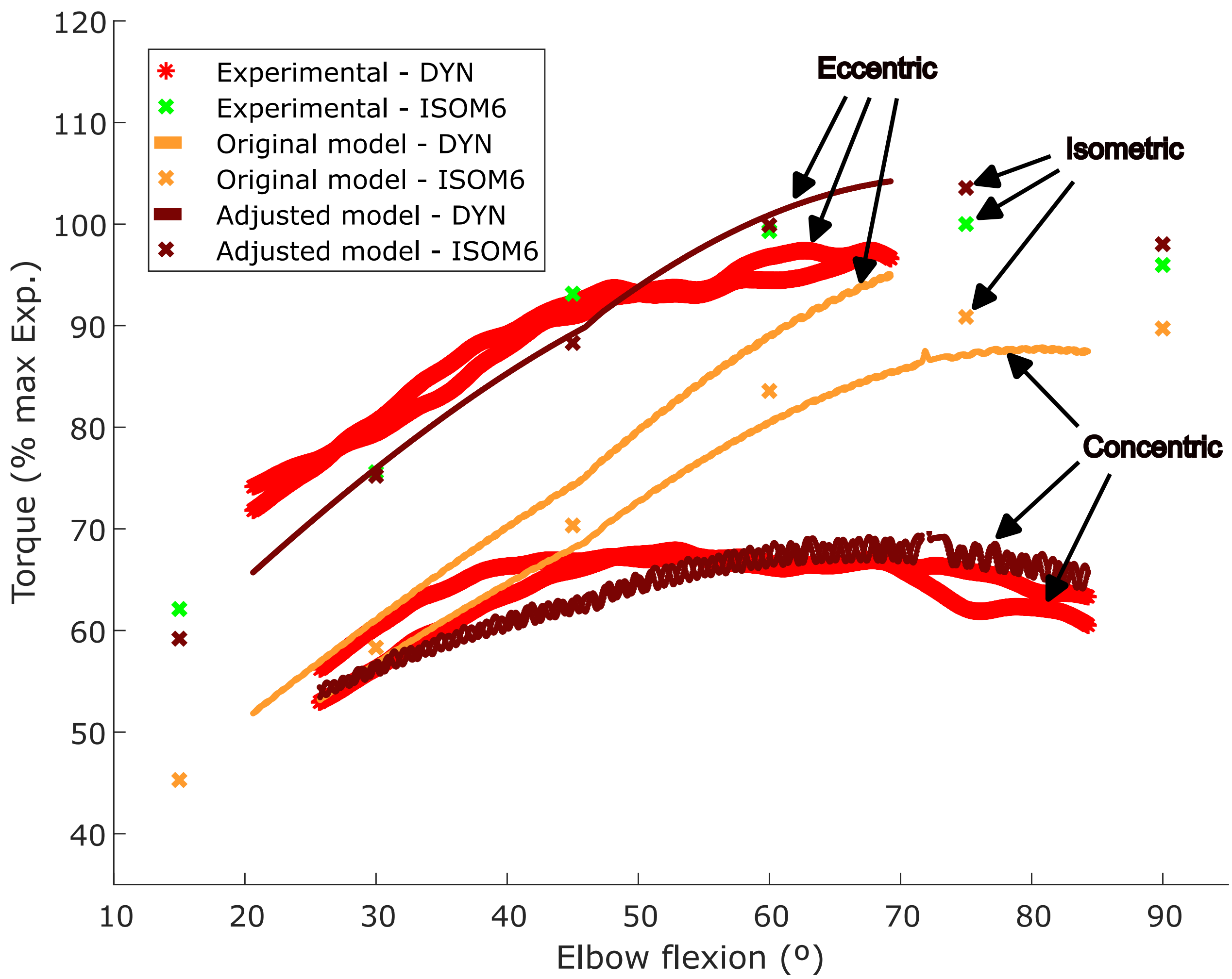

Fig. 3 Preliminary comparison of the estimated torques from the original and adjusted models with experimental measurements for a healthy subject during DYN and ISOM6

shortening effects, whereas eccentric and isometric measurements show similar behavior. At a 60° elbow flexion angle, despite identical musculotendon lengths and moment arms, the maximum force generated during the concentric MVC was 40% lower than that of the eccentric and isometric MVCs due to the force–velocity relationship.

b. The maximum possible value of $f_v(v^M)$ during eccentric task, is typically set to 1.4 for young adults [50]. Given that $f_v(0) = 1$ during isometric task, as spotlighted in Fig. 3 with the original model, the eccentric maximum forces should theoretically be 40% higher. However, neither our experimental measurements nor the results at different speeds reported in [49] confirmed this increase at the elbow joint.

As a result, the following two model adjustments were implemented to enhance MTU force estimation:

a. With its default parameter values, the Hill muscle model failed to accurately capture the MTU force-length and force-velocity relationships, even after scaling l_0^M, as the formulation of $f_v(v^M)$ did not accurately represent the force-velocity dependency. The force-velocity relationship is expressed in terms of the normalized MTU fiber velocity $\widetilde{v}^M$, which is defined as:

$$\widetilde{v}^M = \frac{v^M}{v_{\max}} \tag{11}$$

where $v_{\max}$ is the maximum contraction velocity, calculated as $v_{\max} = \frac{l_0^M}{\tau_c}$. The parameter τ_c is known as the time-scaling parameter, and is tipically set to 0.1 s for all MTUs [32].

However, by adjusting τ_c, the authors observed significant improvements (represented in brown in Fig. 3). Therefore, they decided to include this parameter in the subject-specific optimized calibration.

b. After the first adjustment, the simulation of the dynamic task showed a good match with experimental data; however, isometric tasks were significantly underestimated, since $f_v^{\max}=1.4$. Therefore, we opted to set $f_v^{\max} = 1.01$, which resulted in a stronger correlation for both dynamic and isometric tasks.

To highlight the impact of these adjustments, they were exclusively applied to a single calibration strategy—PHYS3-DYN, detailed in Sect. "Muscle force evaluation without fatigue"—rather than implementing them across all simulations.

Muscle fatigue parameters

As detailed in [29], the parameters F_S and F_L define the fatigue rates, while R_S and R_L define the recovery rates of the short-term and long-term fatigued states, respectively. Additionally, r acts as a multiplier to enhance recovery during rest. The short-duration protocol of [28] was applied, using the isometric experimental measurements during the 30-s sustained MVC at 45° to calibrate the short-term fatigue state parameters (F_S, R_S and r). However, due to the lack of long-duration experimental measurements, the authors adopted default values for the long-term parameters, setting R_L=2e-4 and F_L=4e-4 to induce a slight long-lasting nonmetabolic fatigue.

Model-calibration combinations and evaluation

Muscle force evaluation without fatigue

As observed, numerous MTU parameters can be adjusted, and various calibration strategies are possible. To determine the simplest and most efficient non-invasive technique for musculoskeletal model calibration, this study tested different approaches by combining default and calibrated MTU parameters for two muscle models. The tested approaches are categorized as follows and summarized in Table 1:

Approaches calibrated from isometric measurements:

PHYS1-ISOM1: Only F_0^M of the physiological Hill-musculotendon model was calibrated by applying a single scale factor to all the MTUs derived from a single isometric measurement (ISOM1, MVC at 60°).

PHYS2-ISOM6: Individual F_0^M and l_0^M for the physiological Hill-musculotendon model were calibrated using an optimization technique based on six isometric measurements (ISOM6).

STAT-ISOM6: Individual F_0^M for the simplified musculotendon model were calibrated using an optimization technique based on six isometric measurements (ISOM6).

Approaches calibrated from dynamic measurements:

PHYS1-DYN: Individual F_0^M of the physiological Hill-musculotendon model were calibrated using an optimization technique based on dynamic experimental measurements from the isokinetic calibration task, including both concentric and eccentric contractions.

PHYS2-DYN: Individual F_0^M and l_0^M of the physiological Hill-musculotendon model were calibrated using an optimization technique based on dynamic experimental measurements from the isokinetic calibration task, including both concentric and eccentric contractions.

PHYS3-DYN: Individual F_0^M and l_0^M, and τ_c of the physiological Hill-musculotendon model were calibrated using an optimization technique based on the isokinetic calibration task, including both concentric and eccentric

Table 1 Summary of the approaches implemented in this study

Approaches	Muscle model	Experiment	F_0^M	l_0^M	τ_c	$f_v^{\max}$	Fatigue parameters
PHYS1-ISOM1	Hill muscle model	ISOM1	Scale factor	Scaled from geometry	0.1 s	1.4	Original
PHYS2-ISOM6	Hill muscle model	ISOM6	Optimized	Optimized	0.1 s	1.4	Original
STAT-ISOM6	Static model	ISOM6	Optimized	N.A	N.A	N.A	Original
PHYS1-DYN	Hill muscle model	DYN	Optimized	Scaled	0.1 s	1.4	Original
PHYS2-DYN	Hill muscle model	DYN	Optimized	Optimized	0.1 s	1.4	Original
PHYS3-DYN	Hill muscle model	DYN	Optimized	Optimized	Optimized	1.01	Original
PHYS3-DYN*	Hill muscle model	DYN	Optimized	Optimized	Optimized	1.01	Optimized

contractions. Additionally, $f_v^{\max}$ was set to 1.01 (while set to its default value 1.4 for the others approaches).

The optimization technique (*fmincon*, MATLAB, version R2023a, MathWorks, Natick, MA, USA) aimed to achieve the best fit between the model and experimental results by allowing F_0^M to vary from 50 to 150% of its original cadaver-derived value and l_0^M to range from 90 to 120% of its pre-scaled value. Finally, τ_c limits were set between 1/15 s and 2 s.

As an indicator, the optimizations were conducted on a computer equipped with an Intel(R) Core(TM) i7-13700KF @ 3.40 GHz processor, 32 GB of RAM, and a 2 TB SSD running Windows 10 Pro. All calibrations were performed using a single-threaded program written in Matlab, which required less than 15 s per subject. Since computational time was not a significant factor, no specific comparison was conducted.

To compare these six approaches, the root mean square error (RMSE) was calculated between the elbow torques produced by the MTU forces estimated in each approach and the experimental measurements. This evaluation was performed separately for isometric tasks (ISOM6) and dynamic tasks (DYN). A paired-sample t-test was performed for each pair of approaches to statistically compare their differences. Prior to applying the t-tests, the normality of the paired RMSE differences was verified using the Kolmogorov–Smirnov test (after standardizing the differences), and no violations of the normality assumption were detected. To control the increased risk of Type I error due to multiple comparisons, a Bonferroni correction was applied [51]. Specifically, 15 pairwise comparisons were conducted (corresponding to all combinations of 6 approaches), and each p-value was adjusted accordingly.

Muscle force evaluation with fatigue

In this work, since the evaluated task was intended to be performed at MVC, two different hypothesis were considered for simulating muscle force and fatigue during DYN-FAT:

Option (a): Assuming $TL = 100\%$ and $a = 1$, based on the premise that participants maintained full MVC throughout the entire exercise.

Option (b): Estimating TL and activation level a from experimental measurements, by calculating the ratio between the experimentally measured torque and the estimated maximum torque the MTUs could generate. To avoid introducing the complexity of the force-sharing problem and the need to simulate individual muscle fatigue, a uniform activation level was applied across all MTUs at the joint level.

The differences between the two approaches affected all time steps, as any variation in MTU activation or target load leads to a different muscle fatigue time history. In this study, option (a) was tested using MTU parameters previously calibrated with the STAT-ISOM6, PHYS2-DYN, and PHYS3-DYN approaches to simulate maximum force and fatigue during DYN-FAT. Then, option (b) was tested using only the PHYS3-DYN approach, which demonstrated the best performance in this study.

Muscle force evaluation with fatigue considering maximum target load (option a) The STAT-ISOM6, PHYS2-DYN, and PHYS3-DYN approaches were applied to simulate maximum force and fatigue development during the dynamic, short-duration, high-intensity exercise (DYN-FAT). As described in Sect. "Muscle fatigue model", the muscle fatigue model was integrated into the musculotendon model to account for task-specific fatigue during dynamic movement. The generic model parameters from the previous 3CC muscle compartment model [52], which does not account for long-term muscle fatigue, were used to simulate short-term muscle fatigue. Therefore, the parameters were set as follows: $F_S = 0.00912$, $R_S = 0.00094$, $r = 15$. For the long-term fatigue component, the parameters were set to $F_L = 0.0004$ and $R_L = 0.0002$.

To further evaluate the effect of subject-specific calibration of the fatigue parameters, the authors combined the calibrated fatigue parameters (Sect. "Muscle fatigue parameters") with the PHYS3-DYN muscle model, resulting in a new protocol referred to as PHYS3-DYN*.

To evaluate these four calibrations, the RMSE was computed by comparing the elbow torques generated by the estimated flexor MTU forces at maximum contraction ($a = 1$ and $TL = 100\%$) with the experimental measurements. Additionally, in order to highlight the effects of these discrepancies on the determination of the target load (TL), the RMSE was calculated between the expected TL (100%) and the estimated TL^*, which was determined using the following equation based on the estimated torque (Q_{Sim}^{Max}) and the experimental torque (Q_{Exp}):

$$TL* = \frac{Q_{Exp}}{Q_{Sim}^{Max}} \tag{12}$$

for the non-physiological approach, and,

$$TL* = \frac{Q_{Exp} - Q_{Sim,PE}}{Q_{Sim}^{Max} - Q_{Sim,PE}} \tag{13}$$

for the physiological approach, where $Q_{Sim,PE}$ is the torque generated by the passive element, so as to isolate the ratio of torques corresponding solely to the contractile element. In both cases, TL^* was limited to 100% when $Q_{Sim}^{Max} < Q_{Exp}$. To provide a statistical comparison, paired-sample t-test was also performed for each pair of approaches to statistically compare their differences.

Muscle force evaluation with fatigue from estimated target load (option b) To assess the accuracy of the best of the previous approaches (PHYS3-DYN) in a scenario where TL is not predefined (option b) and remains unknown, we used the estimated target load based on torques proportion (TL^{**}) to determine the corresponding MTU activations ($a = TL^{**}/100$). A uniform activation level was applied across all MTUs at the joint level to avoid introducing the force-sharing problem and the need to simulate individual muscle fatigue. TL^{**} was calculated similarly to TL^{*} (Eq. 13), but it reflects the fatigue time history specific to this scenario. The corresponding torques and fatigue levels were computed at each time step. The RMSE was then calculated by comparing the elbow torque generated by the estimated MTU forces with the experimental measurements.

Results

Muscle force evaluation without fatigue

The different approaches proposed in this study were evaluated by comparing the estimated torques with the experimentally measured torques from seventeen healthy subjects during isometric and dynamic MVCs. Figure 4 illustrates the maximum isometric torques of the elbow flexors for a healthy subject, estimated using all approaches during ISOM6. The simplest calibration approach, PHYS-ISOM1, accurately matched the torque only at the 60° angle, where it was calibrated. Additionally, PHYS1-DYN (sky blue) and PHYS2-DYN (green) tended to underestimate isometric tasks. The non-physiological approach (STAT-ISOM6) did not accurately replicate the shape of the experimental data (red). PHYS2-ISOM6 and PHYS3-DYN demonstrated the highest reliability, as confirmed by the mean values presented in Table 2, with mean RMSE across subjects for the six ISOM6 tasks of 5.4 and 7.5%, respectively. Moreover, paired t-tests conducted between the different approaches revealed significant differences in almost all pairwise comparisons, except for PHYS1-ISOM1 and STAT-ISOM6, which showed similar results (see Table 3). Among all methods,

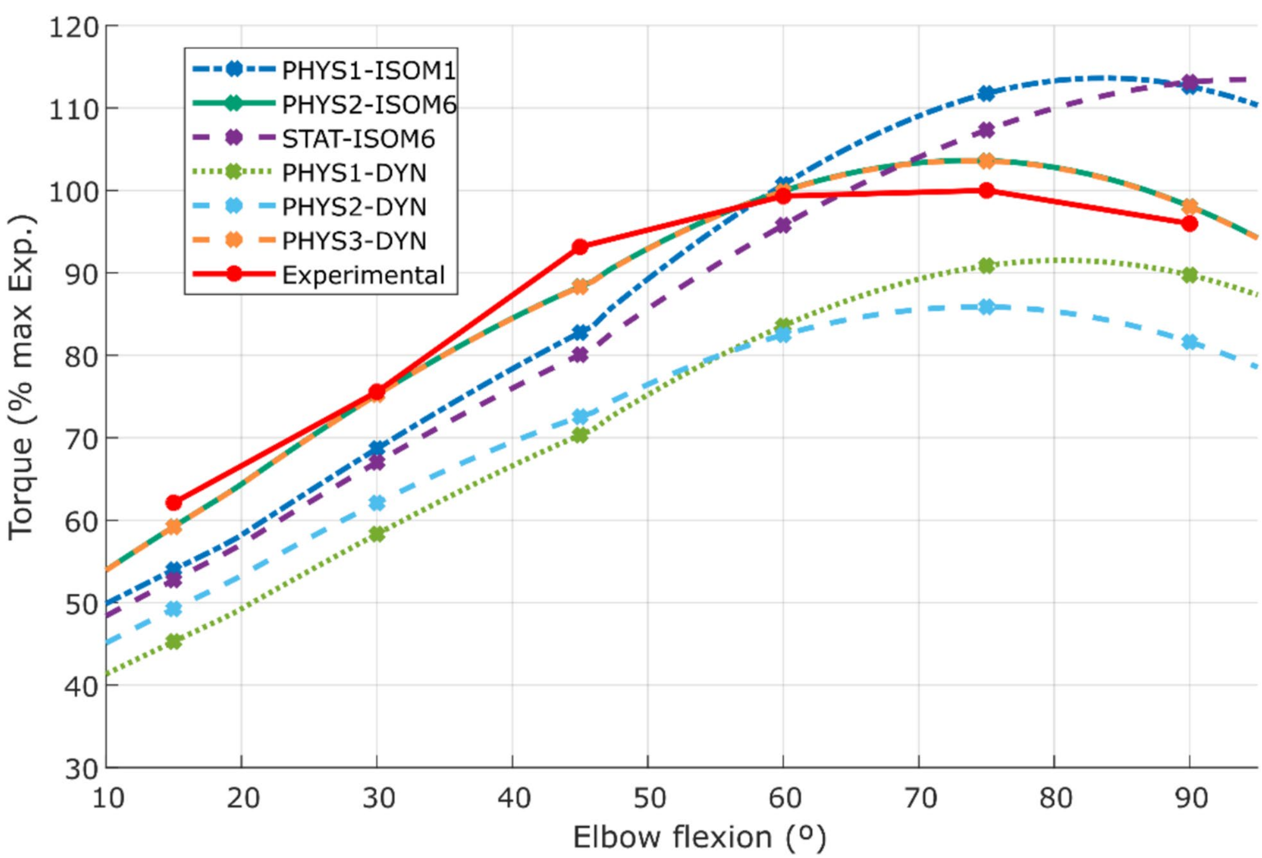

Fig. 4 Maximum isometric torques of elbow flexors estimated with the different approaches versus experimental (red) for a healthy subject during ISOM6

Table 2 Mean RMSE across subjects of the multiple approaches during ISOM6 and DYN (RMSE < 10% in bold)

		Mean Torque Estimation RMSE (%) of Multiple Approaches During ISOM6 and DYN Conditions, with ± Standard Deviation					
		PHYS1-ISOM1	PHYS2-ISOM6	STAT-ISOM6	PHYS1-DYN	PHYS2-DYN	PHYS3-DYN
ISOM6	15º	18.0 ± 9.0	10.6 ± 7.7	18.9 ± 7.8	31.1 ± 9.3	24.4 ± 10.0	**12.3 ± 9.1**
	30º	**9.0 ± 8.9**	**5.2 ± 4.9**	**9.9 ± 6.9**	22.3 ± 7.0	16.7 ± 7.1	**5.5 ± 5.7**
	45º	**8.7 ± 5.8**	**4.2 ± 3.7**	**7.2 ± 5.3**	17.2 ± 7.0	14.3 ± 6.4	**6.2 ± 4.9**
	60º	**2.4 ± 2.9**	**3.5 ± 3.1**	**5.5 ± 4.2**	16.0 ± 6.4	16.6 ± 5.9	**5.9 ± 4.9**
	75º	12.0 ± 9.4	**4.8 ± 3.9**	**7.6 ± 5.7**	10.2 ± 6.4	14.4 ± 6.0	**6.7 ± 4.3**
	90º	14.0 ± 9.4	**4.4 ± 4.7**	14.6 ± 9.1	10.7 ± 5.7	17.2 ± 7.4	**8.3 ± 6.2**
	Mean	10.7 ± 5.3	**5.4 ± 2.6**	10.6 ± 5.1	17.9 ± 7.9	17.3 ± 3.7	**7.5 ± 2.5**
DYN		21.3 ± 6.0	18.8 ± 3.4	21.2 ± 3.1	12.3 ± 2.3	10.5 ± 2.2	**4.5 ± 1.6**

Table 3 Bonferroni-corrected *p*-values from paired sample *t*-tests comparing torque RMSE between modeling approaches across subjects during ISOM6 ($p > 0.05$ in bold, N.A.: not applicable)

	Bonferroni-corrected *p*-values from paired sample *t*-tests comparing RMSE of the multiple approaches across subjects during ISOM6					
	PHYS1-ISOM1	PHYS2-ISOM6	STAT-ISOM6	PHYS1-DYN	PHYS2-DYN	PHYS3-DYN
PHYS1-ISOM1	N.A	< 0.01	**13.60**	< 0.01	< 0.01	0.03
PHYS2-ISOM6	< 0.01	N.A	< 0.01	< 0.01	< 0.01	0.01
STAT-ISOM6	**13.60**	< 0.01	N.A	< 0.01	< 0.01	**0.07**
PHYS1-DYN	< 0.01	< 0.01	< 0.01	N.A	**0.57**	< 0.01
PHYS2-DYN	< 0.01	< 0.01	< 0.01	**0.57**	N.A	< 0.01
PHYS3-DYN	0.03	0.01	**0.07**	< 0.01	< 0.01	N.A

the least accurate estimation occurred at 15°, when the elbow was in its most extended position.

Figure 5 presents the maximum concentric and eccentric torques of the elbow flexors for one healthy subject, estimated using all approaches during DYN. Approaches calibrated using ISOM6 data showed good fidelity with experimental data (red) only during eccentric tasks, resulting in the highest RMSE, with values around 20% (Table 2). In contrast, approaches calibrated using DYN data aimed to match both eccentric and concentric tasks, yielding better overall results. PHYS3-DYN provided the best solution, with a mean RMSE of 4.5% across subjects for dynamic tasks and significant differences compared to its counterparts (see Table 4).

Muscle force evaluation with fatigue

Muscle force evaluation with fatigue considering maximum target load (option a)

The different approaches in this study were evaluated by comparing the estimated maximum torque of the elbow flexors ($TL = 100\%$ and $a = 1$ for flexors) with the experimentally measured torque from seventeen healthy subjects during a dynamic, short-duration, high-intensity exercise, where fatigue was expected. Figure 6 illustrates the estimated torques for a healthy subject, estimated using all approaches described in Sect. "Muscle force evaluation with fatigue", during the two concentric and two eccentric elbow flexion cycles (DYN-FAT) and the two isometric recovery measurements (DYN-FAT-R1 and DYN-FAT-R2). The STAT-ISOM6 approach showed poor agreement with experimental data, particularly during concentric phases. In contrast, PHYS3-DYN and PHYS3-DYN* exhibited high accuracy across all phases of the exercise. Their results were largely similar, except for a notable difference in recovery behavior observed in this subject. PHYS2-DYN yielded more accurate results than STAT-ISOM6, though it did not reach the level of precision achieved by PHYS3-DYN and PHYS3-DYN. These findings are summarized in Table 5, which presents the mean RMSE across subjects for both dynamic and isometric (recovery measurements) tasks. The mean errors for PHYS3-DYN and PHYS3-DYN* were 15.0% and 14.8%, respectively, for the dynamic task and approximately 10% for the isometric MVC during recovery. Conversely,

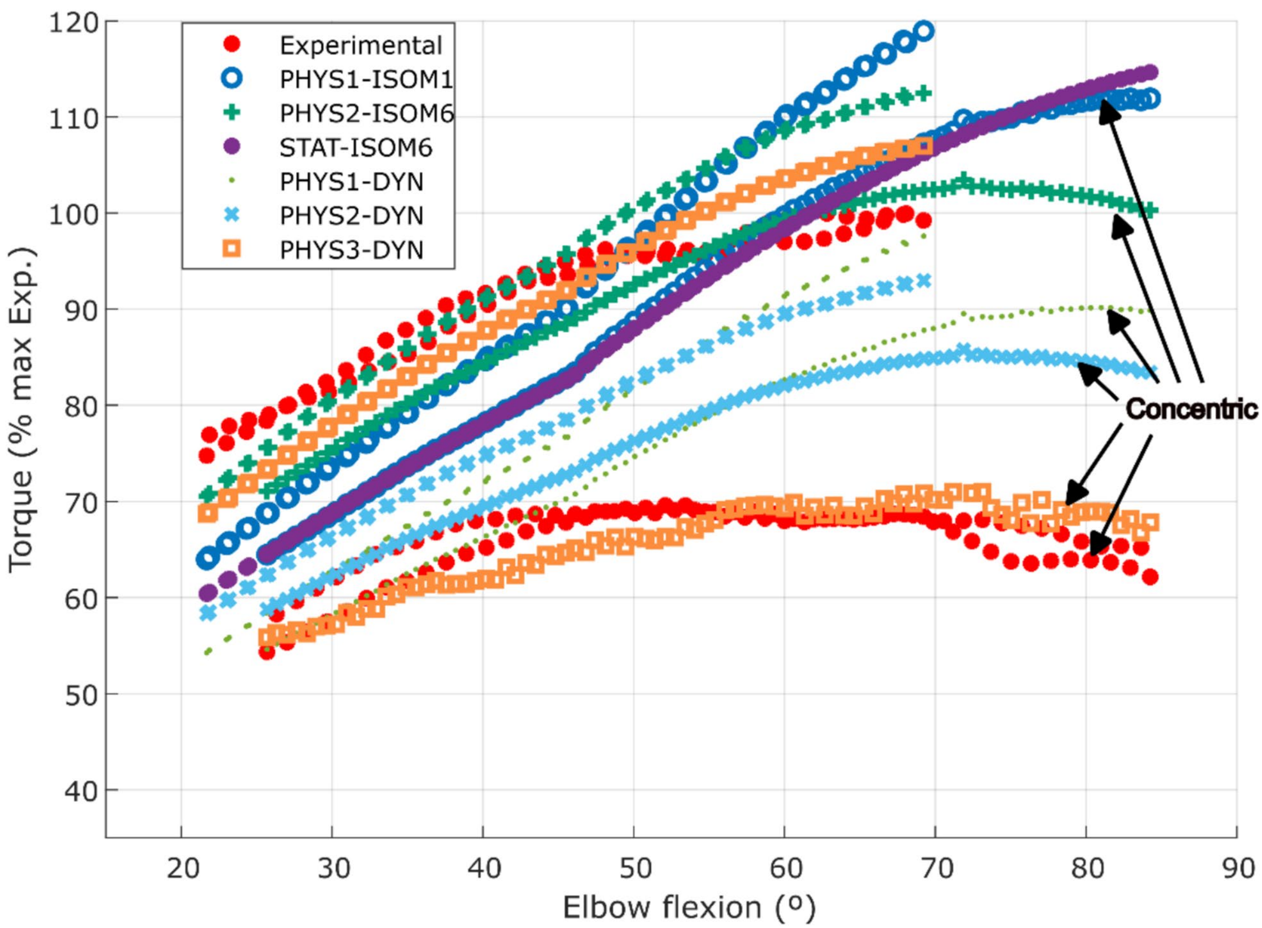

Fig. 5 Maximum dynamic (concentric and eccentric) torques of elbow flexors estimated with the different approaches versus experimental (red) for a healthy subject during DYN

Table 4 Bonferroni-corrected *p*-values from paired sample *t*-tests comparing torque RMSE between modeling approaches across subjects during DYN (p > 0.05 in bold, N.A.: not applicable)

	Bonferroni-corrected *p*-values from paired sample *t*-tests comparing torque RMSE of the multiple approaches across subjects during DYN					
	PHYS1-ISOM1	**PHYS2-ISOM6**	**STAT-ISOM6**	**PHYS1-DYN**	**PHYS2-DYN**	**PHYS3-DYN**
PHYS1-ISOM1	N.A	**0.42**	**14.11**	< 0.01	< 0.01	< 0.01
PHYS2-ISOM6	**0.42**	N.A	< 0.01	< 0.01	< 0.01	< 0.01
STAT-ISOM6	**14.11**	< 0.01	N.A	< 0.01	< 0.01	< 0.01
PHYS1-DYN	< 0.01	< 0.01	< 0.01	N.A	< 0.01	< 0.01
PHYS2-DYN	< 0.01	< 0.01	< 0.01	< 0.01	N.A	< 0.01
PHYS3-DYN	< 0.01	< 0.01	< 0.01	< 0.01	< 0.01	N.A

STAT-ISOM6 yielded the poorest results, with an average RMSE of 25.5% during the dynamic task. The discrepancies in torque estimations closely mirrored those observed in the estimated target load (TL^*). The p-values from the paired-sample t-tests presented in Table 6 indicate that PHYS3-DYN and PHYS3-DYN* do not exhibit significant differences between them. However, both approaches show statistically superior performance compared to the other methods.

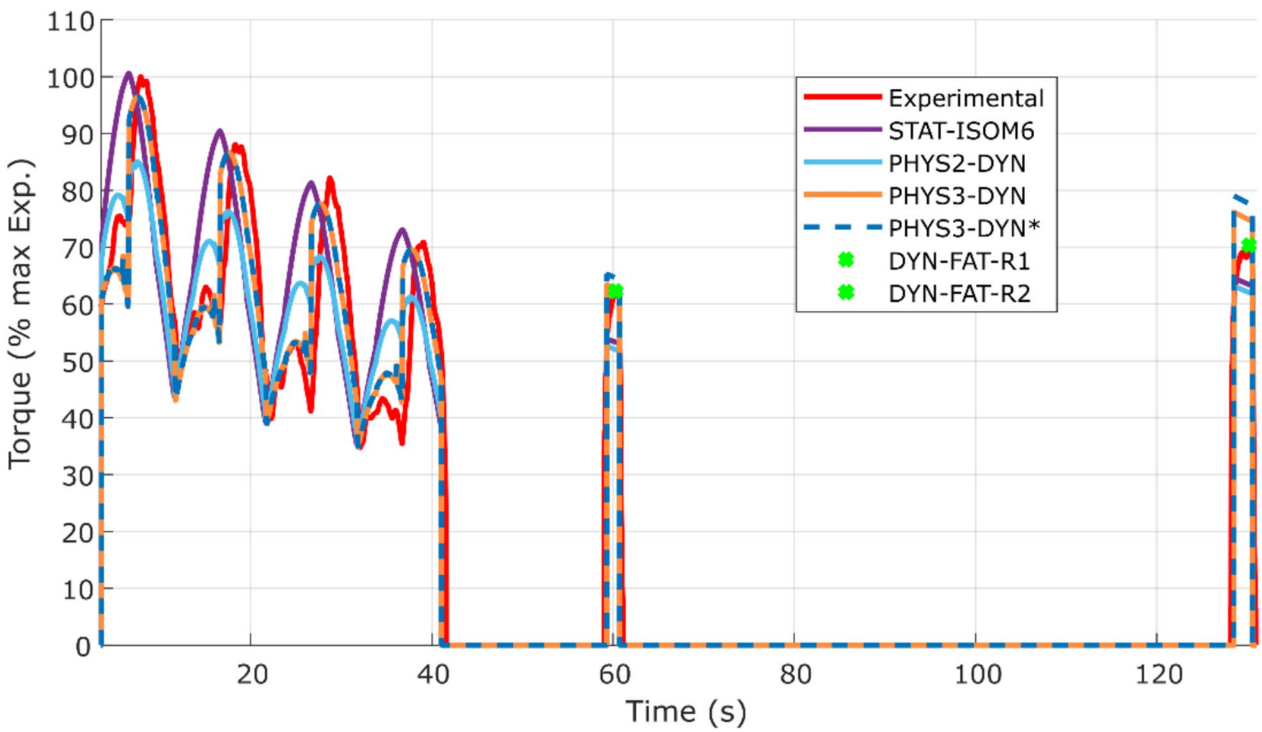

Fig. 6 Maximum dynamic and isometric fatigued torques of elbow flexors estimated with the different approaches versus experimental (red) for a single subject during DYN-FAT, DYN-FAT-R1 and DYN-FAT-R2

Table 5 Mean torque estimation RMSE (%) for multiple approaches during DYN-FAT, with ± standard deviation (RMSE < 10% in bold)

	Mean torque estimation RMSE (%) for multiple approaches during DYN-FAT, with ± standard deviation			
	STAT-ISOM6	PHYS2-DYN	PHYS3-DYN	PHYS3-DYN*
DYN-FAT	25.5 ± 4.4	16.2 ± 3.6	15.0 ± 4.5	14.8 ± 4.2
DYN-FAT-R1	11.9 ± 9.3	17.4 ± 10.4	**9.3 ± 10.1**	10.9 ± 10.2
DYN-FAT-R2	**8.6 ± 6.4**	12.2 ± 9.5	**9.2 ± 7.4**	10.0 ± 7.1
TL	26.1 ± 4.1	16.1 ± 3.8	15.4 ± 4.1	15.2 ± 3.6

Table 6 Bonferroni-corrected *p*-values from paired sample *t*-tests comparing torque RMSE of the multiple approaches across subjects during DYN-FAT (p > 0.01 in bold, N.A.: not applicable)

	Bonferroni-corrected *p*-values from paired sample *t*-tests comparing torque RMSE of the multiple approaches across subjects during DYN-FAT (including DYN-FAT-R1 and DYN-FAT-R2)			
	STAT-ISOM6	PHYS2-DYN	PHYS3-DYN	PHYS3-DYN*
DYN-FAT	N.A	**13.87**	< 0.01	< 0.01
DYN-FAT-R1	**13.87**	N.A	0.01	0.02
DYN-FAT-R2	< 0.01	0.01	N.A	**4.77**
TL	< 0.01	0.02	**4.77**	N.A

Evaluation of muscle force with fatigue from estimated target load (option b)

Finally, Fig. 7 illustrates the dynamic and isometric fatigued torques of the elbow flexors when evaluating the accuracy of PHYS3-DYN by estimating the target load (TL^{**}, in black) and MTU activation based on the experimentally measured torque for a single subject. When $TL^{**} = 100\%$, the simulated torque corresponds to the maximum torque. As TL^{**} decreases, the estimated torques are adjusted by reducing MTU activity to align with the experimental values. The mean RMSE across subjects for torques and for target load estimation (with an experimental $TL = 100\%$) during DYN-FAT were 7.62 and 15.85%, respectively.

Discussion

This study aims to improve muscle force and fatigue estimation during dynamic, short-duration, high-intensity exercise by comparing different muscle models and calibration strategies. Two musculotendon models were analyzed: a Hill-type model with a rigid tendon, which includes physiological force constraints, and a

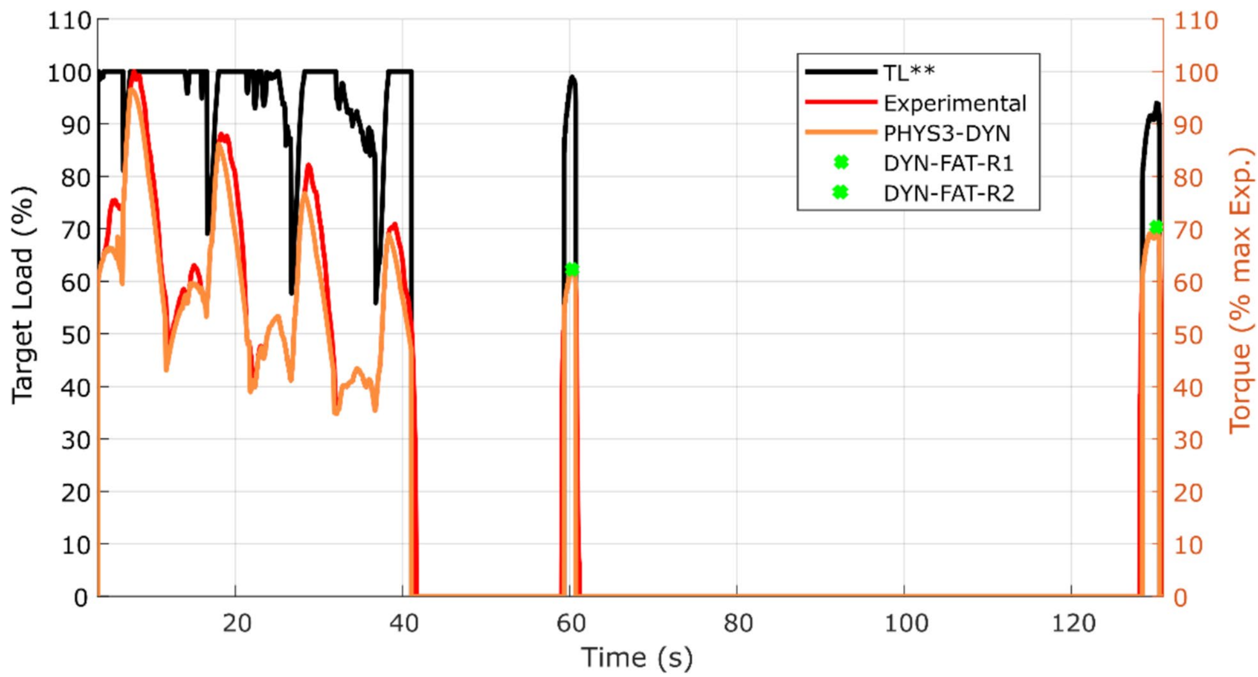

Fig. 7 Dynamic and isometric fatigued torque of elbow flexors (orange) and target load (black) estimated with PHYS3-DYN versus experimental (red) for a single subject during DYN-FAT, DYN-FAT-R1 and DYN-FAT-R2

simplified static model that ignores musculotendon actuator dynamics. After scaling a generic model using anthropometric data, different force calibration strategies were tested based on isometric and isokinetic measurements from an isokinetic dynamometer. Additionally, the impact of further fatigue model calibration was evaluated. Finally, each calibration strategy was applied to estimate muscle forces and fatigue, and the results were compared, taking as reference the experimental measurements, to determine the most effective approach.

The PHYS-ISOM1 calibration approach accurately matched the torque at 60°, the angle used for its calibration, but showed significant discrepancies at other elbow angles, resulting in the highest RMSE during the dynamic task. This finding underscores the importance of implementing subject-specific calibration of generic models to achieve more physiologically accurate musculotendon mechanics, as recommended in [16]. While calibrating MTU parameters from isometric MVCs at multiple positions, as done in [27, 28], improved force estimation for isometric and eccentric MVCs, it failed to account for musculotendon length-velocity shortening effects during concentric contractions. Similarly, while calibrating MTU parameters from dynamic MVCs improved force estimation for concentric tasks, PHYS1-DYN and PHYS2-DYN tended to underestimate isometric tasks due to the maximum value of the dimensionless force–velocity relationship, $f_v^{\max}$, being originally set to 1.4 for young adults [50]. However, neither the authors' experimental measurements, nor the results at different speeds reported in [49], confirmed this increase at the elbow joint during eccentric tasks. In addition, the authors statistically demonstrated that the two additional adjustments to the original Hill-muscle model, proposed in Sect. "Additional force–length-velocity properties", significantly enhanced muscle force estimation, ensuring high accuracy across isometric, eccentric, and concentric tasks at elbow level. The least accurate estimation of isometric MVCs occurred when the elbow was most extended (15°). The authors suggest that experimental measurements may have been biased by additional elbow flexion caused by the soft support of the dynamometer, or by shoulder flexion, as the elbow position was not adequately stabilized, which could have interfered with elbow flexion and affected measurement accuracy.

Although the simplified static model has shown good performance in gait analysis [42], the results obtained during high-intensity elbow flexion revealed its significant limitations. While the isometric MVC estimations from the STAT-ISOM6 approach may be acceptable, the model's limited physiological representation hinders its ability to accurately simulate the force–velocity relationship during concentric movements in dynamic tasks.

When estimating MTU forces during dynamic, short-duration, high-intensity exercise, where fatigue was expected, the authors emphasized the challenges of integrating an efficient muscle fatigue model within the multibody system dynamics framework for human movement analysis. They highlighted that these difficulties cannot be fully evaluated without experimental data, which was omitted in [53]. A poor physiological representation of the musculotendon model and an inadequate calibration may result in poor estimations of the maximum MTU forces, leading primarily to an underestimated target load, which directly impacts muscle fatigue predictions. Additionally, this miscalculation affects force distribution, posing further challenges in addressing the force-sharing problem [28]. PHYS3-DYN, the method with improved MTU force calibration, showed the best estimation and did not show significant improvement when using subject-specific calibrated muscle fatigue model parameters. It could significate that adjusting these parameters is not crucial, or that the proposed protocol to calibrate them was not efficient.

In this work, the authors successfully estimated isometric, eccentric, and concentric muscle forces with fatigue at the elbow joint using an efficient, non-invasive calibration protocol, both at a known maximum target load and by estimating muscle activity and target load from the torque and muscular capacity. It is important to note that performing MVCs, particularly dynamic and sustained MVCs, can be challenging for subjects, meaning some discrepancies may also arise from brief decreases in exerted intensity. This work utilized an isokinetic dynamometer, but the authors believe that any system capable of recording varying joint angle during maximum force could be suitable, and maintaining a constant velocity should not be a strict requirement. The study utilized the 4CC muscle fatigue model [29], provided objective estimations and accounted for eccentric contractions, unlike [30]. This fatigue model not only integrates seamlessly into the multibody system dynamics and MTU actuator dynamics frameworks, but also facilitates its application in muscle force-sharing problems, which requires simulating individual muscle fatigue [28].

One limitation of this study lies in the use of the dynamometer which, despite being specifically designed for isolated joint force measurements, does not fully constrain the elbow joint. Minor compensatory movements, such as wrist or shoulder flexion, or unintended additional elbow flexion, may occur due to the compliant nature of the soft support. This, combined with the inherent difficulty for participants to maintain true MVC, especially over extended periods and under fatigue, limits the ability to obtain perfectly accurate results. Electromyography measurements could have provided additional insights, particularly regarding MTU activation levels and potential co-contractions. A second limitation of this study is its focus on a single joint—the elbow—with only one degree of freedom. While this restricts the immediate generalizability of the findings, the choice was intentional. The musculoskeletal model was deliberately aligned with the simplicity of the experimental setup to create a controlled and interpretable environment for evaluating complex calibration strategies and muscle modeling approaches. By minimizing biomechanical complexity, we aimed to reduce confounding factors and isolate the effects of model calibration. Despite the simplicity of the joint-level representation, the study revealed significant challenges in achieving physiologically accurate estimations of muscle force and fatigue. These insights form a critical foundation for extending the methodology to more complex, multi-joint models in future work. Particular attention should be given to the calibration of multi-articulate muscles, which play a key role in coordinating movement across multiple joints and present additional challenges in parameter estimation [54].

In future work, the authors plan to evaluate the relationship between maximum eccentric and isometric torque to refine the dimensionless force–velocity relationship ($f_v^{\max}$) for different joints. Additionally, having previously validated the 4CC muscle fatigue model independent of MTU dynamics [29] and now confirming the calibration of MTU dynamics both with and without fatigue, the authors plan to integrate this calibration protocol and fatigue modeling into their real-time human motion capture, reconstruction, and musculoskeletal analysis framework to simulate any physical activity [39].

Conclusion

This study highlights the importance of precise MTU calibration and demonstrates that accurately estimating MTU force during high-intensity, short-duration exercise is best achieved using a physiological Hill-type muscle model with carefully calibrated individual parameters F_0^M and l_0^M from concentric and eccentric MVCs, alongside adjustments to the force–velocity relationship (PHYS3-DYN). However, adding subject-specific fatigue parameters does not significantly improve force prediction under fatigued conditions.

Abbreviations

α	Pennation angle
a	Muscle activation
f_l	Dimensionless force–length relationship of the active element
f_v	Dimensionless force–velocity relationship
$f_v^{\max}$	Maximum normalized achievable muscle force when the muscle is lengthening
f_{PE}	Dimensionless force–length relationship of the passive element
F_S	Short-term fatigue coefficient
F_L	Long-term fatigue coefficient
F_{CE}^M	Force exerted by the contractile element

$F^{M}_{CE,Max}$	Maximum force allowed by the contractile element
F^{M}_{PE}	Force exerted by the passive element
F^{M}_{0}	Maximum isometric force
F^{Flex}	Flexor muscle force
F^{Ext}	Extensor muscle force
F^{MT}_{Stat}	Non-physiological (static) estimation of muscle force
$\mathbf{F}^{MT}$	The vector of the individual musculotendon forces
$\mathbf{J}$	Jacobian whose transpose projects the muscle forces into the joint drive torques space
l^{M}	Muscle fiber length
l^{M}_{0}	Optimal muscle fiber length
l^{MT}	Musculotendon length
l^{T}_{S}	Tendon slack length
M_a	Percentage of motor units activated
M_f	Percentage of motor units fatigued
M^{S}_{f}	Percentage of motor units affected by short-term fatigue
M^{L}_{f}	Percentage of motor units affected by long-term fatigue
M_r	Percentage of motor units resting
Q	Joint torque
Q_{Exp}	Experimental joint torque
r	Rest multiplier to augment recovery during rest
R	Recovery coefficient
R_S	Short-term fatigue recovery coefficient
R_L	Long-term fatigue recovery coefficient
RC	Portion of maximum force available
TL	Target load
τ_c	Time-scaling parameter
v^{M}	Contractile element velocity
$\widetilde{v}^{M}$	Normalized muscle fiber velocity
$v_{\max}$	Maximum contraction velocity
v^{MT}	Musculotendon velocity
3CC	Three-compartment controller model
4CC	Four-compartment controller model to predict metabolic inhibition and long-lasting nonmetabolic components
DYN	Dynamic experimental measurements from the isokinetic calibration task, including both concentric and eccentric contractions
DYN-FAT	Dynamic, short-duration, high-intensity exercise with fatigue
DYN-FAT-R1	Isometric MVCs at 45° to measure the recovery after resting 15 s
DYN-FAT-R2	Isometric MVCs at 45° to measure the recovery after resting 60 s
ISOM1	Single experimental measurement of isometric MVC at 60°
ISOM6	Six static experimental measurements of isometric MVCs
MVC	Isometric maximum voluntary contraction3
MTU	Muscle tendon unit
PHYS1-ISOM1	Only F^{M}_{0} of the physiological Hill-musculotendon model was calibrated by applying a single scale factor to all the muscles derived from a single isometric measurement (ISOM1, MVC at 60°)
PHYS2-ISOM6	Individual F^{M}_{0} and l^{M}_{0} of the physiological Hill-musculotendon model were calibrated using an optimization technique based on six isometric measurements (ISOM6)
STAT-ISOM6	Individual F^{M}_{0} of the non-physiological musculotendon model were calibrated using an optimization technique based on six isometric measurements (ISOM6)
PHYS1-DYN	Individual F^{M}_{0} of the physiological Hill-musculotendon model were calibrated using an optimization technique based on dynamic experimental measurements from the isokinetic calibration task, including both concentric and eccentric contractions.
PHYS2-DYN	Individual F^{M}_{0} and l^{M}_{0} of the physiological Hill-musculotendon model were calibrated using an optimization technique based on dynamic experimental measurements from the isokinetic calibration task, including both concentric and eccentric contractions.
PHYS3-DYN	Individual F^{M}_{0} and l^{M}_{0}, and τ_c of the physiological Hill-musculotendon model were calibrated using an optimization technique based on the isokinetic calibration task, including both concentric and eccentric contractions. Additionally, $f^{\max}_{v}$ was set to 1.01 (while set to its default value 1.4 for the others approaches).
PHYS3-DYN*	PHYS3-DYN combined with subject-specific calibration of the fatigue parameters.
RMSE	Root mean square error.

Acknowledgements
Authors would like to acknowledge the subjects for their voluntary participation in this project.

Author contributions
F.M. and G.M. designed the experiments with the supervision of M.G-G and J.C. F.M. and G.M. performed the experiments with the help of M.G-G. F.M. derived the models and analyzed the data. F.M. wrote the original draft. G.M, M.G-G and J.C. reviewed and edited the manuscript. J.C. oversaw project administration and funding acquisition.

Funding
Authors would like to acknowledge the different funding supports. Grant PID2022-140062OB-I00 funded by MCIN/AEI/10.13039/501100011033 and by "ERDF A way of making Europe", by the European Union. Grant ED431C 2023/01 by the Galician Government. Moreover, F. Michaud would like to acknowledge the support of the Galician Government and the Ferrol Industrial Campus by means of the postdoctoral research contract 2022/CP/048.

Data availability
The datasets generated for this study are available on reasonable request to the corresponding author.

Declarations

Ethical approval and consent to participate
The studies involving human participants were reviewed and approved by the Research Ethics Committee of La Coruña-Ferrol. The participants provided their written informed consent to participate in this study.

Consent for publication
The participants provided their written informed consent for publication.

Competing interests
The authors declare no competing interests.

Received: 11 April 2025 Accepted: 1 July 2025
Published online: 10 July 2025

References

1. Fregly BJ. A Conceptual Blueprint for Making Neuromusculoskeletal Models Clinically Useful. Appl Sci. 2021;11(5):2037. https://doi.org/10.3390/app11052037.
2. Michaud F, Serrancolí G, Quental C, Innocenti B. Editorial: advances in the neuromusculoskeletal modeling of injuries, diseases, and clinical treatments. Front Neurosci. 2024. https://doi.org/10.3389/fnins.2024.1463130.
3. Scherb D, Wartzack S, Miehling J. Modelling the interaction between wearable assistive devices and digital human models—a systematic review. Front Bioeng Biotechnol. 2023. https://doi.org/10.3389/fbioe.2022.1044275.
4. Bulat M, Korkmaz Can N, Arslan YZ, Herzog W. Musculoskeletal Simulation Tools for Understanding Mechanisms of Lower-Limb Sports Injuries. Curr Sports Med Rep. 2019;18(6):210–6. https://doi.org/10.1249/JSR.0000000000000601.
5. Noteboom L, Belli I, Hoozemans MJM, Seth A, Veeger HEJ, Van Der Helm FCT. Effects of bench press technique variations on musculoskeletal shoulder loads and potential injury risk. Front Physiol. 2024. https://doi.org/10.3389/fphys.2024.1393235.

6. Li G, et al. Changes in walking function and neural control following pelvic cancer surgery with reconstruction. Front Bioeng Biotechnol. 2024. https://doi.org/10.3389/fbioe.2024.1389031.
7. Febrer-Nafría M, Nasr A, Ezati M, Brown P, Font-Llagunes JM, McPhee J. Predictive multibody dynamic simulation of human neuromusculoskeletal systems: a review. Multibody Syst Dyn. 2023;58(3–4):299–339. https://doi.org/10.1007/s11044-022-09852-x.
8. Roberts TJ, Gabaldon AM. Interpreting muscle function from EMG: lessons learned from direct measurements of muscle force. Integr Comp Biol. 2008;48(2):312–20. https://doi.org/10.1093/icb/icn056.
9. Lee S, Park M, Lee K, Lee J. Scalable muscle-actuated human simulation and control. ACM Trans Graph. 2019;38(4):1–13. https://doi.org/10.1145/3306346.3322972.
10. Zhang X, Chan FK, Parthasarathy T, Gazzola M. Modeling and simulation of complex dynamic musculoskeletal architectures. Nat Commun. 2019;10(1):4825. https://doi.org/10.1038/s41467-019-12759-5.
11. Richter H, Warner H. Motion optimization for musculoskeletal dynamics: a flatness-based polynomial approach. IEEE Trans Automat Contr. 2021;66(7):3289–95. https://doi.org/10.1109/TAC.2020.3029318.
12. Chen Z, Franklin DW. Musculotendon Parameters in Lower Limb Models: simplifications, Uncertainties, and Muscle Force Estimation Sensitivity. Ann Biomed Eng. 2023;51(6):1147–64. https://doi.org/10.1007/s10439-023-03166-5.
13. Scovil CY, Ronsky JL. Sensitivity of a Hill-based muscle model to perturbations in model parameters. J Biomech. 2006;39(11):2055–63. https://doi.org/10.1016/j.jbiomech.2005.06.005.
14. Ackland DC, Lin Y-C, Pandy MG. Sensitivity of model predictions of muscle function to changes in moment arms and muscle–tendon properties: a Monte-Carlo analysis. J Biomech. 2012;45(8):1463–71. https://doi.org/10.1016/j.jbiomech.2012.02.023.
15. Lund ME, Andersen MS, de Zee M, Rasmussen J. Scaling of musculoskeletal models from static and dynamic trials. Int Biomech. 2015;2(1):1–11. https://doi.org/10.1080/23335432.2014.993706.
16. Akhundov R, et al. Is subject-specific musculoskeletal modelling worth the extra effort or is generic modelling worth the shortcut? PLoS ONE. 2022;17(1):1–16. https://doi.org/10.1371/journal.pone.0262936.
17. Modenese L, Ceseracciu E, Reggiani M, Lloyd DG. Estimation of musculotendon parameters for scaled and subject specific musculoskeletal models using an optimization technique. J Biomech. 2016;49(2):141–8. https://doi.org/10.1016/j.jbiomech.2015.11.006.
18. Luis I, Afschrift M, De Groote F, Gutierrez-Farewik EM. Evaluation of musculoskeletal models, scaling methods, and performance criteria for estimating muscle excitations and fiber lengths across walking speeds. Front Bioeng Biotechnol. 2022. https://doi.org/10.3389/fbioe.2022.1002731.
19. Rakshit R, Yang J. Modelling muscle recovery from a fatigued state in isometric contractions for the ankle joint. J Biomech. 2020;100: 109601. https://doi.org/10.1016/j.jbiomech.2020.109601.
20. Barman S, Xiang Y, Rakshit R, Yang J. Joint fatigue-based optimal posture prediction for maximizing endurance time in box carrying task. Multibody Syst Dyn. 2022. https://doi.org/10.1007/s11044-022-09832-1.
21. Xu Y, et al. Rehabilitation effects of fatigue-controlled treadmill training after stroke: a rat model study. Front Bioeng Biotechnol. 2020. https://doi.org/10.3389/fbioe.2020.590013.
22. de Sire A, et al. Impact of Rehabilitation on Fatigue in Post-COVID-19 patients: a systematic review and meta-analysis. Appl Sci. 2022;12(17):8593. https://doi.org/10.3390/app12178593.
23. Mongrain É, Blanchette A, Ouellet M-C, Amoura SS, Bouffard J. Interactions between fatigue and motor rehabilitation following a stroke: a qualitative study of rehabilitation professionals' perspectives. Arch Phys Med Rehabil. 2021;102(10): e23. https://doi.org/10.1016/j.apmr.2021.07.523.
24. McClean ZJ, et al. A biopsychosocial model for understanding training load, fatigue, and musculoskeletal sport injury in university athletes: a scoping review. J Strength Cond Res. 2024;38(6):1177–88. https://doi.org/10.1519/JSC.0000000000004789.
25. Edwards WB. Modeling overuse injuries in sport as a mechanical fatigue phenomenon. Exerc Sport Sci Rev. 2018;46(4):224–31. https://doi.org/10.1249/JES.0000000000000163.
26. Rousseau T, Venture G, Hernandez V. Latent space representation of human movement: assessing the effects of fatigue. Sensors. 2024;24(23):7775. https://doi.org/10.3390/s24237775.
27. MullerA et al. Non-invasive techniques for musculoskeletal model calibration. In 23ème Congrès Français de Mécanique 2017. p. hal01524330.
28. Michaud F, Frey-Law LA, Lugrís U, Cuadrado L, Figueroa-Rodríguez J, Cuadrado J. Applying a muscle fatigue model when optimizing load-sharing between muscles for short-duration high-intensity exercise: a preliminary study. Front Physiol. 2023. https://doi.org/10.3389/fphys.2023.1167748.
29. Michaud F, Beron S, Lugrís U, Cuadrado J. Four-compartment muscle fatigue model to predict metabolic inhibition and long-lasting nonmetabolic components. Front Physiol. 2024. https://doi.org/10.3389/fphys.2024.1366172.
30. Yang J, Rakshit R, Barman S, Xiang Y. A four-compartment controller model of muscle fatigue for static and dynamic tasks. Front Physiol. 2025. https://doi.org/10.3389/fphys.2025.1518847.
31. Thelen DG. Adjustment of muscle mechanics model parameters to simulate dynamic contractions in older adults. J Biomech Eng. 2003;125(1):70–7. https://doi.org/10.1115/1.1531112.
32. Zajac FE. Muscle and tendon: properties, models, scaling, and application to biomechanics and motor control. Crit Rev Biomed Eng. 1989;17:359–411.
33. Sartori M, Farina D, Lloyd DG. Hybrid neuromusculoskeletal modeling to best track joint moments using a balance between muscle excitations derived from electromyograms and optimization. J Biomech. 2014;47(15):3613–21. https://doi.org/10.1016/j.jbiomech.2014.10.009.
34. Serrancolí G, et al. Neuromusculoskeletal model calibration significantly affects predicted knee contact forces for walking. J Biomech Eng. 2016;138(8):1–11. https://doi.org/10.1115/1.4033673.
35. Ao D, Vega MM, Shourijeh MS, Patten C, Fregly BJ. EMG-driven musculoskeletal model calibration with estimation of unmeasured muscle excitations via synergy extrapolation. Front Bioeng Biotechnol. 2022. https://doi.org/10.3389/fbioe.2022.962959.
36. Arones MM, Shourijeh MS, Patten C, Fregly BJ. Musculoskeletal model personalization affects metabolic cost estimates for walking. Front Bioeng Biotechnol. 2020. https://doi.org/10.3389/fbioe.2020.588925.
37. Romdhani A, et al. Exploring the impact of verbal encouragement on strength, endurance, and psychophysiological responses: enhancing teaching strategies in sports science education. Front Sport Act Living. 2024. https://doi.org/10.3389/fspor.2024.1360717.
38. Saul KR, et al. Benchmarking of dynamic simulation predictions in two software platforms using an upper limb musculoskeletal model. Comput Methods Biomech Biomed Engin. 2015;18(13):1445–58. https://doi.org/10.1080/10255842.2014.916698.
39. Lugrís U, Pérez-Soto M, Michaud F, Cuadrado J. Human motion capture, reconstruction, and musculoskeletal analysis in real time. Multibody Syst Dyn. 2023. https://doi.org/10.1007/s11044-023-09938-0.
40. Millard M, Uchida T, Seth A, Delp SL. Flexing computational muscle: modeling and simulation of musculotendon dynamics. J Biomech Eng. 2013. https://doi.org/10.1115/1.4023390.
41. Van Campen A, Pipeleers G, De Groote F, Jonkers I, De Schutter J. A new method for estimating subject-specific muscle-tendon parameters of the knee joint actuators: a simulation study. Int J Numer Method Biomed Eng. 2014;30(10):969–87. https://doi.org/10.1002/cnm.2639.
42. Michaud F, Lamas M, Lugrís U, Cuadrado J. A fair and EMG-validated comparison of recruitment criteria, musculotendon models and muscle coordination strategies, for the inverse-dynamics based optimization of muscle forces during gait. J Neuroeng Rehabil. 2021. https://doi.org/10.1186/s12984-021-00806-6.
43. Gandevia SC. Spinal and supraspinal factors in human muscle fatigue. Physiol Rev. 2001;81(4):1725–89. https://doi.org/10.1152/physrev.2001.81.4.1725.
44. WallmannH. Muscle Fatigue. In Sports-Specific Rehabilitation, Elsevier, 2007. p. 87–95. https://doi.org/10.1016/B978-044306642-9.50008-3.
45. Carroll TJ, Taylor JL, Gandevia SC. Recovery of central and peripheral neuromuscular fatigue after exercise. J Appl Physiol. 2017;122(5):1068–76. https://doi.org/10.1152/japplphysiol.00775.2016.
46. Frey-Law LA, Looft JM, Heitsman J. A three-compartment muscle fatigue model accurately predicts joint-specific maximum endurance times for

sustained isometric tasks. J Biomech. 2012;45(10):1803–8. https://doi.org/10.1016/j.jbiomech.2012.04.018.
47. Sartori M, Reggiani M, Farina D, Lloyd DG. EMG-driven forward-dynamic estimation of muscle force and joint moment about multiple degrees of freedom in the human lower extremity. PLoS ONE. 2012;7(12): e52618. https://doi.org/10.1371/journal.pone.0052618.
48. Documentation O. Working with Static Optimization. https://simtk-confluence.stanford.edu:8443/display/OpenSim/Working+with+Static+Optimization
49. Komi PV, Linnamo V, Silventoinen P, Sillan M. Force and EMG power spectrum during eccentric and concentric actions. Med Sci Sport Exerc. 2000;32(10):1757–62. https://doi.org/10.1097/00005768-200010000-00015.
50. Thelen DG, Anderson FC, Delp SL. Generating dynamic simulations of movement using computed muscle control. J Biomech. 2003;36(3):321–8. https://doi.org/10.1016/S0021-9290(02)00432-3.
51. Curtin F, Schulz P. Multiple correlations and bonferroni's correction. Biol Psychiatry. 1998;44(8):775–7. https://doi.org/10.1016/S0006-3223(98)00043-2.
52. Looft JM, Herkert N, Frey-Law L. Modification of a three-compartment muscle fatigue model to predict peak torque decline during intermittent tasks. J Biomech. 2018;77:16–25. https://doi.org/10.1016/j.jbiomech.2018.06.005.
53. PereiraAF, Silva MT, Martins JM, De Carvalho M. Implementation of an efficient muscle fatigue model in the framework of multibody systems dynamics for analysis of human movements. Proc Inst Mech Eng Part K J Multi-body Dyn. 2011;225(4):359–370. https://doi.org/10.1177/1464419311415954.
54. Miyake T, Okabe M. Roles of Mono- and Bi-articular Muscles in Human Limbs: two-joint Link Model and Applications. Integr Org Biol. 2022. https://doi.org/10.1093/iob/obac042.

Publisher's Note